IOP PUBLISHING JOURNAL OF PHYSICS D: APPLIED PHYSICS

J. Phys. D: Appl. Phys. **41** (2008) 245205 (11pp) doi:10.1088/0022-3727/41/24/245205

Monte Carlo studies of non-conservative electron transport in the steady-state Townsend experiment

S Dujko[1,2], R D White[2] and Z Lj Petrović[1]

[1] Institute of Physics, University of Belgrade, PO Box 68, Zemun, Belgrade, Serbia
[2] ARC Centre for Antimatter-Matter Studies, School of Mathematics, Physics and Information Technology, James Cook University, Townsville 4810, Australia

E-mail: sasa.dujko@jcu.edu.au

Received 30 July 2008, in final form 22 September 2008
Published 27 November 2008
Online at stacks.iop.org/JPhysD/41/245205

Abstract
An investigation of the spatial relaxation of the electrons and benchmark calculations of spatially resolved non-conservative electron transport in model gases has been carried out using a Monte Carlo simulation technique. The Monte Carlo code has been specifically developed to study the spatial relaxation of electrons in an idealized steady-state Townsend (SST) experiment in the presence of non-conservative collisions. Calculations have been performed for electron transport properties with the aim of providing the benchmark required to verify the codes used in plasma modelling. Both the spatially uniform values and the relaxation profiles of the electron transport properties may serve as an accurate test for such codes. The explicit effects of ionization and attachment on the spatial relaxation profiles are considered using physical arguments. We identify the relations for the conversion of hydrodynamic transport properties to those found in the SST experiment. Our Monte Carlo simulation code and sampling techniques appropriate to these experiments have provided us with a way to test these conversion formulae and their convergence.

1. Introduction

In recent years the study of spatially resolved electron kinetics in neutral gases under the action of an electric field has gained in importance for development and further optimization of plasma sources used in the plasma processing industry [1]. One of the major challenges in this area is an understanding of the spatial variations and related relaxation processes of the electron transport properties in atomic and molecular gases. This essentially non-hydrodynamic behaviour is often labelled in the physics of non-equilibrium plasmas as non-local (or transient) behaviour. The spatial variations of the electron transport properties can be caused by various mechanisms. These include the local disturbances of the electron velocity distribution function, electron transport in rapidly varying fields in space and/or time, the presence of external sources of ionization, electron transport at very high electric field to gas number density ratio (E/n_0) or electron transport near emitting or absorbing physical boundaries such as electrodes, enclosing walls, internal grids and probes. A number of theoretical methods to calculate the electron transport properties under these 'non-hydrodynamic' conditions, especially those attempting to model or simulate the cathode fall of a dc [2] or sheath of rf discharges [3], revealed the non-local nature of electron transport. The failure of the hydrodynamic approximation and the spatial non-locality of electron transport has been recognized and marked as one of the biggest difficulties in the early development of plasma models [4, 5]. A survey of various kinetic problems and difficulties occurring in inhomogeneous plasma regions, their approximate kinetic treatment and range of applicability prior to the 1990s has been reviewed in [6].

More recently, the modern non-hydrodynamic kinetic studies on the electron spatial relaxation revealed the complex nature of the relaxation process and associated basic mechanisms. The groups at Griefswald (Winkler and co-workers) and James Cook University (Robson and co-workers) attract special attention. Unlike others, who directly applied their methods to treat complex plasma phenomena in various inhomogeneous plasma regions, they focused on

the half-range free space problems including the modelling of an idealized steady-state Townsend (SST) experiment with the aim of understanding the fundamental mechanisms of the spatial relaxation of electron ensemble properties. Winkler and co-workers employed a two-term, Legendre polynomial representation of the velocity distribution for solving the Boltzmann equation to study the field free spatial relaxation of the electrons and related spatially decaying plasma phenomena [7], spatial relaxation of the electrons in uniform [8–11] and non-uniform [12] electric fields, spatial relaxation in spatially periodic fields [13–15] and response of the electrons to spatial disturbance of the electric field [11, 16]. A two-term representation of the distribution function in spherical harmonics has been applied for a treatment of both the non-local electron kinetics in the anode region [17] and radially inhomogeneous electron kinetics [18]. The two-term theory has been extended to a multi-term treatment of spatial relaxation in spatially uniform fields [19], and spatial relaxation in the cathode [20, 21] and anode [22] regions of a glow discharge. Similar kinetic studies on spatial relaxation of the electrons in uniform and spatially periodic fields have been performed by Golubovskii *et al* [23–26]. For atomic systems, it may be anticipated that the two-term analysis is of sufficient accuracy, but in general, a multi-term representation of the distribution function, in full spherical harmonics, not just Legendre polynomials, is required [27]. This was the program carried out by Robson and co-workers in an attempt to study the effects of non-conservative collisions on spatial relaxation of the electrons [28], using a two-temperature moment method, whereby the spatial dependence was treated by both finite difference and eigenfunction techniques. However, the spectrum of problems associated with spatial relaxation processes of the electrons is even larger. In that respect, the effect of electron–electron interactions [29] and effects of a magnetic field [30, 31] on spatial relaxation of the electrons have been investigated.

The conclusions emerging from the previous studies of Winkler and co-workers and Robson and co-workers are consistent with each other and may be summarized as follows. The nature of the spatial relaxation profiles of the electron transport properties is dependent on the interplay between the power dissipated in elastic collisional processes, power dissipated in threshold collisional processes and the power dissipated into the swarm by the field [28, 32, 33]. For certain gases, there exists a 'window' of E/n_0 strengths where the relaxation profiles are damped oscillatory in nature, and outside this window the profiles are monotonic. The seminal experiment of Franck and Hertz, as discussed recently by Robson *et al* [33] and Sigeneger *et al* [34], was the first to provide evidence of these effects, while Holst–Oosterhuis periodic luminous layers observed in rare gas discharges are also a manifestation of these phenomena [35]. The non-intrusive photon flux experiment of Fletcher [36] and Malović *et al* [37, 38] provides a means of directly observing the periodic structures of electron transport properties common to all the above arrangements, which for present purposes can be classified as variations on the SST experiment. However, in spite of these well-known illustrative examples, the spatial variations and associated relaxation phenomena of the electron transport properties have been difficult to quantify experimentally on a systematic basis because of their dependence on initial and experimental conditions. Moreover, in the swarm experiments used for measurement of the electron transport coefficients and determination of low-energy electron–molecule cross sections, both theoretical and experimental work has been carried out to avoid/minimize the detrimental action of non-hydrodynamic phenomena in order to obtain more reliable hydrodynamic transport properties [39]. One such example is separation of the delay distance and the hydrodynamic exponential growth in SST experiments and analysis of the Paschen curve [40] or measurement of excitation coefficients.

In understanding physically the spatial variations of the electron transport parameters, the Monte Carlo simulations and the flight-time integral method (FTI) have also played an important role. The group led by Tagashira has demonstrated the differences in the electron transport properties due to the methods of observation, pulsed Townsend (PT), SST and time of flight (TOF) following the previous work of Thomas [41] and proposed the way of sampling of spatially resolved electron transport data under SST conditions [42, 43]. Boeuf and Marode employed a Monte Carlo simulation technique to study the spatial dependence of the electron transport parameters in a strong electronegative gas SF_6, and showed that these parameters may be position dependent throughout the gap between electrodes [44]. The non-hydrodynamic effects at high values of E/n_0 when both runaway and boundary effects are significant throughout the discharge were studied by Stojanović and Petrović in nitrogen [45] and argon [46]. Sugawara and co-workers improved the propagator method of Sommerer [47] and applied this method for calculation of SST spatially uniform electron transport data [48, 49]. Finally, the steady-state Townsend flight time integral (SST–FTI) method has been employed for the similar studies of the spatially resolved energy distribution function and electron transport properties in CF_4 [50].

The aim of this paper is to present a systematic analysis of the effect of non-conservative collisions (ionization/attachment) on the spatial relaxation profiles using a Monte Carlo simulation technique. The results of the analysis and their physical interpretation are presented for certain model gases. The motivations for using the Monte Carlo method and model cross sections in benchmark calculations are not always fully appreciated. A Monte Carlo method is based on the first principles without imposing various approximations and boundary conditions on the electron distribution function in velocity space which although convenient from the numerical and mathematical point of view, are often unphysical. The errors in Monte Carlo simulation are essentially of statistical nature only and therefore well understood. Other possible sources of error are oversimplification in representing important phenomena, inaccurate input data or inadequate or statistically biased sampling. Using simple analytic forms of cross sections, however, we can isolate and elucidate fundamental physical processes which govern the spatial variations of the electron transport properties with various

input parameters. In addition, the analytical form of the cross sections provides no ambiguity and uncertainty generated by the complicated structure of real cross sections. Therefore, it is desirable and useful to apply a Monte Carlo method to perform benchmark calculations of spatially dependent electron kinetics and related spatial relaxation processes. To our knowledge, there exist only a limited number of such investigations. Kortshagen *et al* [51] applied a Monte Carlo code as a benchmark tool for testing the so-called 'non-local approximation', a method for solving the space-dependent Boltzmann equation. The influence of the electron attachment process on swarm characteristics under SST conditions in $Ar:NF_3$ mixture has been recently studied through a Boltzmann equation analysis and Monte Carlo simulation by Dyatko *et al* [52]. In order to verify the complex relaxation processes of the electrons studied using two-term [53] and multi-term [22] solutions of the Boltzmann equation, comparative Monte Carlo calculations have also been performed. These illustrative examples are very welcome steps in the right direction but some additional calculations may be required to include more fundamental aspects of spatial relaxation of the electrons, particularly when attempting to fully understand the influence of non-conservative collisions. The role of elastic and inelastic collisions and their energy losses have also been investigated in spatial relaxation of the electrons in this paper. This is the avenue we explore in this work.

The starting point is a brief presentation of our Monte Carlo simulation code specifically developed to model an idealized SST experiment. Rather than present the full review of the simulation technique, we highlight some important points associated with the technique under the SST conditions and refer the reader to [4, 54] for a detailed discussion of standard Monte Carlo procedures. We also introduce a new scheme to calculate the expansion coefficients in density gradient expansions of average transport properties in the hydrodynamic regime. This yields hydrodynamic transport properties such as the flux drift velocity, flux diffusion tensor and gradient energy parameter. We are then able to represent SST transport properties in terms of these general quantities calculated under hydrodynamic conditions. One of the primary purposes here is to use Monte Carlo simulations to test these hydrodynamic expansions under SST conditions, their convergence and range of applicability. In order to achieve this goal, two different sampling techniques for spatially dependent electron transport data have been developed and employed in our code. Sampling of hydrodynamic transport properties in infinite electron swarms is well defined for both dc and ac electric fields when non-conservative collisions are operative. However, most experiments deal with SST conditions where at any particular point along the discharge there exist electrons originating from the cathode at different times. In particular, it is difficult to obtain both space and time resolved data under these conditions, and hence an important aspect of this work is to give an outline of sampling techniques appropriate to SST experiments. The background of these sampling techniques is a rigorous kinetic theory and this is clearly demonstrated in this work. Finally, we pay particular attention to the influence of non-conservative collisions (ionization/attachment) on spatial relaxation profiles. We have presented the importance of treating ionization in a correct way as the non-conservative collisional processes rather than as other inelastic processes for the determination of spatial relaxation processes. In this paper we make a further generalization with respect to the work of Li *et al* [28] to consider the explicit effects of the electron attachment collisional processes on spatial profiles of the electron transport data.

2. On the connection between SST transport properties and transport coefficients

2.1. Distribution functions, hydrodynamic regime and transport coefficients

The behaviour of a swarm of electrons in gases under the influence of electric and magnetic fields can be described by the time evolution of the phase-space distribution function $f(\boldsymbol{r}, \boldsymbol{v}, t)$ where $\boldsymbol{r}$ and $\boldsymbol{v}$ define co-ordinates in position and velocity space respectively. The phase-space distribution function is defined such that $f(\boldsymbol{r}, \boldsymbol{v}, t)\,\mathrm{d}\boldsymbol{r}\,\mathrm{d}\boldsymbol{v}$ is the number of particles within $\mathrm{d}\boldsymbol{r}$ of $\boldsymbol{r}$ and $\mathrm{d}\boldsymbol{v}$ of $\boldsymbol{v}$ at time t. The phase-space distribution function can be determined from solution of the Boltzmann equation or from a Monte Carlo simulation. Quantities of interest can be determined from the appropriate integrals over velocity and/or configuration space. For example, the average value of the property φ at a given position is defined as

$$\langle\varphi\rangle = \frac{\int \varphi f(\boldsymbol{r}, \boldsymbol{v}, t)\,\mathrm{d}\boldsymbol{v}}{\int f(\boldsymbol{r}, \boldsymbol{v}, t)\,\mathrm{d}\boldsymbol{v}} = \frac{1}{n(\boldsymbol{r}, t)}\int \varphi f(\boldsymbol{r}, \boldsymbol{v}, t)\,\mathrm{d}\boldsymbol{v}, \tag{1}$$

where $n(\boldsymbol{r}, t)$ is the number density at that position. The mean value of the same property over the entire swarm is

$$\tilde{\varphi} = \frac{\int \varphi f(\boldsymbol{r}, \boldsymbol{v}, t)\,\mathrm{d}\boldsymbol{r}\,\mathrm{d}\boldsymbol{v}}{\int f(\boldsymbol{r}, \boldsymbol{v}, t)\,\mathrm{d}\boldsymbol{r}\,\mathrm{d}\boldsymbol{v}} = \frac{1}{N}\int \varphi f(\boldsymbol{r}, \boldsymbol{v}, t)\,\mathrm{d}\boldsymbol{r}\,\mathrm{d}\boldsymbol{v}, \tag{2}$$

where N is the total number of swarm particles.

The experimentally measurable quantities in swarm experiments are usually the charged particle currents or charged particle densities. The connection between experiment and theory can be made through the equation of continuity

$$\frac{\partial n(\boldsymbol{r}, t)}{\partial t} + \nabla \cdot \Gamma(\boldsymbol{r}, t) = S(\boldsymbol{r}, t), \tag{3}$$

where $\boldsymbol{\Gamma}(\boldsymbol{r}, t) = n\langle\boldsymbol{v}\rangle$ is the swarm particle flux and $S(\boldsymbol{r}, t)$ represents the production rate per unit volume per unit time arising from non-conservative collisional processes. We are following the conventional definitions of transport coefficients and assume that the hydrodynamic approximation pertains, so that all space–time dependence is expressible through linear functionals of $n(\boldsymbol{r}, t)$ [39]. A sufficient representation is a density gradient expansion of the phase-space distribution function [39]:

$$f(\boldsymbol{r}, \boldsymbol{v}, t) = \sum_{s=0}^{\infty} \boldsymbol{f}^{(s)}(\boldsymbol{v}) \otimes (-\nabla)^{(s)} n(\boldsymbol{r}, t), \tag{4}$$

where the following normalization condition is satisfied

$$\int f^{(s)}(\boldsymbol{v})\,\mathrm{d}\boldsymbol{v} = \delta_{s0}. \tag{5}$$

Substitution of (4) into (1) yields the density gradient expansion of $\langle\varphi\rangle(\boldsymbol{r},t)$. The density gradient expansion of the average energy and average velocity are

$$\varepsilon(\boldsymbol{r},t) = \sum_{s=0}^{\infty}\varepsilon_s(-\nabla)^s n = \tilde{\varepsilon} + \gamma\cdot\frac{\nabla n}{n} + \cdots, \tag{6}$$

$$\boldsymbol{v}(\boldsymbol{r},t) = \sum_{s=0}^{\infty}\Gamma_s(-\nabla)^s n = \boldsymbol{W}^{(\star)} - \frac{1}{n}\boldsymbol{D}^{(\star)}\cdot\nabla n + \cdots, \tag{7}$$

where

$$\varepsilon_s = \int \frac{1}{2}mv^2 f^{(s)}(\boldsymbol{v})\,\mathrm{d}\boldsymbol{v}, \tag{8}$$

$$\Gamma_s = \int v f^{(s)}(\boldsymbol{v})\,\mathrm{d}\boldsymbol{v}. \tag{9}$$

Here $\tilde{\varepsilon}$ is the mean energy and $\gamma = -n\varepsilon_1$ is the gradient energy parameter [55], $\boldsymbol{W}^{(\star)}$ and $\boldsymbol{D}^{(\star)}$ define, respectively, the flux drift velocity and flux diffusion tensor. Performing equivalent representations of the flux $\boldsymbol{\Gamma}(\boldsymbol{r},t)$ and source term $S(\boldsymbol{r},t)$ (to the orders shown), we have

$$\boldsymbol{\Gamma}(\boldsymbol{r},t) = \boldsymbol{W}^{(\star)}n(\boldsymbol{r},t) - \boldsymbol{D}^{(\star)}\cdot\nabla n(\boldsymbol{r},t), \tag{10}$$

$$S(\boldsymbol{r},t) = S^{(0)}n(\boldsymbol{r},t) - S^{(1)}\cdot\nabla n(\boldsymbol{r},t) + \boldsymbol{S}^{(2)}:\nabla\nabla n(\boldsymbol{r},t). \tag{11}$$

Substitution of expansions (10) and (11) into the continuity equation (3) yields the *diffusion equation*,

$$\frac{\partial n}{\partial t} + \boldsymbol{W}\cdot\nabla n - \boldsymbol{D}:\nabla\nabla n = -R_a n, \tag{12}$$

which defines the *bulk* transport coefficients

$$R_a = -S^{(0)} \qquad \text{(loss rate)}, \tag{13}$$

$$\boldsymbol{W} = \boldsymbol{W}^{(\star)} + \boldsymbol{S}^{(1)} \qquad \text{(bulk drift velocity)}, \tag{14}$$

$$\boldsymbol{D} = \boldsymbol{D}^{(\star)} + \boldsymbol{S}^{(2)} \qquad \text{(bulk diffusion tensor)}. \tag{15}$$

In swarm experiments the bulk transport coefficients are generally measured and tabulated. These transport coefficients are associated with the swarm's centre of mass transport. The explicit influence of non-conservative collisional processes on the swarm's centre of mass transport is described by the correction terms $\boldsymbol{S}^{(1)}$ and $\boldsymbol{S}^{(2)}$. Obviously, in the absence of non-conservative processes, these two sets of transport coefficients coincide.

2.2. Transport under SST conditions

In this work we study spatial relaxation of the electron transport properties in an idealized SST experiment with plane-parallel geometry. A steady stream of electrons emitted from the cathode enters and ionizes the gas and at a sufficiently large distance z from the cathode it is usually assumed that $n(z) \approx \exp(\alpha z)$, where α is the first Townsend ionization coefficient [44, 56–58]. In an electron-attaching gas, the electron number density decreases according to the similar exponential law. There exists a steady state in which transport properties are independent of time and vary with the position only. It is generally found that for a region near the cathode/source 'non-hydrodynamic' behaviour exists [43]. In this regime, the continuity equation (3) still holds but representations involving low-order density gradient expansions fail (e.g. diffusion equation) and hence concepts of quantities like diffusion coefficients do not necessarily apply in this region. At sufficient distances from the cathode/source, however, the velocity dependence (and hence average transport properties) does not vary with position and hydrodynamic conditions prevail.

The transport properties of interest in our SST study are the spatial evolution of the average energy and average velocity. Although we are not advocating the use of labels to assign different transport properties to different experiments, for emphasis in this paper we shall use the subscript SST to designate that the properties have relaxed to their spatially independent values, e.g. 'SST average energy' $\varepsilon_{\mathrm{SST}}$ and 'SST average velocity' v_{SST}. Assuming the exponential growth of the electron number density with the distance $n(z) \approx \exp(\alpha z)$, it follows from (6) and (7) that the density gradient expansion of the average energy and average velocity are, respectively,

$$\varepsilon_{\mathrm{SST}} = \sum_{s=0}^{\infty}\varepsilon_s(-\alpha)^s = \tilde{\varepsilon} + \gamma\alpha + \cdots, \tag{16}$$

$$v_{\mathrm{SST}} = \sum_{s=0}^{\infty}\Gamma_s(-\alpha)^s = W^{(\star)} - D_{\mathrm{L}}^{(\star)}\alpha + \cdots, \tag{17}$$

where $D_{\mathrm{L}}^{(\star)}$ is the flux longitudinal diffusion coefficient. From equations (16) and (17) we can see that the SST average energy and SST average velocity can be calculated from the expansion coefficients, ε_s and Γ_s, in the density gradient expansions of the average energy and velocity, respectively.

It is important to clarify a point which is often a source of confusion introduced in part by terminology. *When non-conservative processes are operative, the SST average energy and SST average velocity are different from those determined from hydrodynamic calculations of the mean energy and flux (or bulk) drift velocities, respectively (e.g. often calculated in TOF analysis).* We shall demonstrate this further in section 4. Rather, $\varepsilon_{\mathrm{SST}}$ can be calculated from $\tilde{\varepsilon}$ and γ (plus higher order terms if higher accuracy is required), while v_{SST} can be calculated from $W^{(\star)}$ and $D_L^{(\star)}$ (plus higher order terms if higher accuracy is required). Obviously, in the absence of non-conservative collisions, $\varepsilon_{\mathrm{SST}}$ reduces to $\tilde{\varepsilon}$ while v_{SST} reduces to $W^{(\star)}$.

This paper follows the traditional but rigorous kinetic theory and in this respect strongly supports the conclusions outlined by Robson [56]. Transport coefficients must be independent of the experimental setup from which they were obtained. The true transport coefficients in this sense are the bulk transport coefficients. Other transport 'coefficients' (e.g. v_{SST}) are dependent on the experimental technique and hence are not, strictly speaking, true transport coefficients. Likewise, the flux transport properties are not true transport coefficients as they are not measurable but can only be calculated in hydrodynamic calculations.

3. Monte Carlo method

In the following section we highlight an improved and more efficient sampling for Monte Carlo simulations of the bulk and flux transport coefficients. Following the pioneering works of Sakai *et al* [42, 43] and Bouef and Marode [44], we develop the set of equations appropriate for sampling of the electron transport data in SST Monte Carlo simulations. We also develop a technique to evaluate the expansion coefficients in the density gradient expansion of the average energy and flux. Similar but not identical work was performed independently in the context of high E/n_0 studies [59]. In this reference the SST experiment was also considered, albeit at high E/n_0 where most of the gap between electrodes is in non-equilibrium.

3.1. Overview and basic assumptions

In our Monte Carlo simulation code we follow the trajectories of a large number of electrons (typically 1×10^6–5×10^6) which undergo collisions with background neutral particles. The primary electrons are isotropically released one by one from the cathode surface into the half space with an initial energy ε_0. Any new secondary electrons arising from electron impact ionization events are followed using the following procedure. When an ionization collision occurs, the set of all dynamic properties (the instant of an ionization collision, the position of new electron, the starting energy and velocity) of a secondary electron are placed at the stack. When a primary electron reaches the anode surface or disappears in an attachment collision event, the first available electron from the stack is followed. These secondary electrons from the stack are released isotropically. In an attachment collision the electron is consumed and hence not simulated further. If the stack is empty, the next primary electron is released and the whole procedure repeats. Thermal motion of the background neutral particles and electron–electron interactions are neglected. The electrodes are considered to be perfectly absorbing.

In the present Monte Carlo code the classical equations of electron motion for an electric field only configuration are employed. We follow the evolution of each electron through time steps governed by the mean collision time. These finite time steps are used to solve the integral equation for the collision probability in order to determine the time of the next collision. This can be done using either the null-collision method [60] or the so-called direct integration method [61]. In our code, the latter approach is employed. The number of time steps is determined in such a way as to optimize the performance of the Monte Carlo code with no reduction in the accuracy of the final results. Once the moment of the next collision is established, the nature of the collision is determined by using the relative probabilities of the various collision types. All electron scattering are assumed to be isotropic regardless of the collision nature, specific process and energy.

3.2. The calculation of bulk and flux transport coefficients

In Monte Carlo simulation, the bulk transport coefficients may be determined from the rate of changes of the appropriate averages of the positions of the electron swarm particles, in the *real* space. The number changing reaction rate is defined by

$$\omega^{(0)} = -\alpha = \frac{\mathrm{d}}{\mathrm{d}t}(\ln N), \tag{18}$$

the drift velocity by

$$\omega^{(1)} = \boldsymbol{W} = \frac{\mathrm{d}}{\mathrm{d}t}\langle \boldsymbol{r} \rangle \tag{19}$$

and the diffusion tensor by

$$\omega^{(2)} = \boldsymbol{D} = \frac{1}{2}\frac{\mathrm{d}}{\mathrm{d}t}\langle \boldsymbol{r}^\star \boldsymbol{r}^\star \rangle, \tag{20}$$

where N is the total number of electrons at any time and $\boldsymbol{r}^\star = \boldsymbol{r} - \langle \boldsymbol{r} \rangle$.

In order to use Monte Carlo simulation to determine the flux transport coefficients one may use the approach proposed by Nolan *et al* [62]. They have developed explicit formulae involving distribution functions for the correction terms $S(j)$ ($j = 0, 1, 2, \ldots$) which allow the determination of the flux transport coefficients using (14) and (15). This method requires numerical integration and hence the accuracy of the flux transport coefficients may be affected by the choice of numerical procedure. One may avoid these difficulties using the following simple formulae for the flux drift velocity and flux diffusion tensor components [4, 54, 63]:

$$\boldsymbol{W}^{(\star)} = \left\langle \frac{\mathrm{d}\boldsymbol{r}}{\mathrm{d}t} \right\rangle = \langle \boldsymbol{v} \rangle, \tag{21}$$

$$D_i^{(\star)} = \langle r_i v_i \rangle - \langle r_i \rangle \langle v_i \rangle, \tag{22}$$

where $\boldsymbol{v}$ is the electron velocity and $i = x, y, z$. We shall show below that the procedures adopted by Nolan *et al* [62] and the above formulae are equivalent. It follows from (21) that the flux drift velocity is the mean velocity of the electrons. Formulae (18)–(22) enable direct calculation of both sets of transport coefficients, flux and bulk, in Monte Carlo simulation. Note that the angular brackets denote the averages over all electrons at any moment t. When the hydrodynamic regime is reached, the averages obtained in such a way are independent of time.

Both sets of transport properties/coefficients, flux and bulk, are necessary as input data in plasma modelling. The bulk values should be used for the analysis of the validity of the cross section. On the other hand, the flux values should be calculated using the Boltzmann equation or Monte Carlo simulation and then used as input data in fluid modelling of plasma discharges [64]. However, the distinction between these two sets of transport coefficients has often been ignored in previous work in the plasma modelling community [64]. This has led to a potentially serious mismatch between the input swarm data required and used. Note that only the Boltzmann equation analysis and/or Monte Carlo simulation can resolve any such mismatch, by providing both flux and bulk transport coefficients. A review of these aspects is contained in [64].

3.3. Sampling of spatially resolved transport data

Let us consider a swarm of electrons released at time $t_0 = 0$ at $\boldsymbol{r}_0 = 0$ with a given initial velocity distribution and let $f(\boldsymbol{r}, \boldsymbol{v}, t)$ be the distribution function of the electrons at time t. Distribution function $f(\boldsymbol{r}, \boldsymbol{v}, t)$ can be presented as a sum of Dirac's delta functions:

$$f(\boldsymbol{r}, \boldsymbol{v}, t) = \sum_{k=1}^{N(t)} \delta(\boldsymbol{r}_k(t) - \boldsymbol{r})\delta(\boldsymbol{v}_k(t) - \boldsymbol{v}), \tag{23}$$

where $N(t)$ is the total number of electrons at time t. Integrating $f(\boldsymbol{r}, \boldsymbol{v}, t)$ over time (from $t_0 = 0$ to infinity) we get the steady-state distribution function $f_{\mathrm{SST}}(\boldsymbol{r}, \boldsymbol{v})$ which can be written as

$$\begin{aligned} f_{\mathrm{SST}}(\boldsymbol{r}, \boldsymbol{v}) &= h \int_0^\infty f(\boldsymbol{r}, \boldsymbol{v}, t)\, \mathrm{d}t \\ &= h \sum_{k,l} \frac{1}{|v_{zk}(t_l)|} \delta(x_k(t_l) - x)\delta(y_k(t_l) - y)\delta(\boldsymbol{v}_k(t_l) - \boldsymbol{v}), \end{aligned} \tag{24}$$

where h is the flux normalized to 1, k is the index for all particles of the swarm (from $t_0 = 0$ to infinity) and l is the number of passes of each electron through the plane perpendicular to axis z. Using formula (24), one may obtain any physical parameter ξ of the swarm in SST experiment at the position z in the following way:

$$\langle \xi \rangle_z = \frac{\int \xi f_{\mathrm{SST}}(\boldsymbol{r}, \boldsymbol{v})\, \mathrm{d}x\, \mathrm{d}y\, \mathrm{d}\boldsymbol{v}}{\int f_{\mathrm{SST}}(\boldsymbol{r}, \boldsymbol{v})\, \mathrm{d}x\, \mathrm{d}y\, \mathrm{d}\boldsymbol{v}}. \tag{25}$$

This is the so-called 'membrane's sampling' method as it corresponds to passages through a membrane perpendicular to the axis of the electric field. The electron number density, mean energy and average velocity are defined, respectively, as follows:

$$n(z) = \int f_{\mathrm{SST}}(\boldsymbol{r}, \boldsymbol{v})\, \mathrm{d}x\, \mathrm{d}y\, \mathrm{d}\boldsymbol{v} = h \sum_{k,l} \frac{1}{|v_{zk}(t_l)|}, \tag{26}$$

$$\varepsilon(z) = \left(\sum_{k,l} \frac{1}{|v_{zk}(t_l)|} \right)^{-1} \sum_{k,l} \frac{\varepsilon_k(t_l)}{|v_{zk}(t_l)|}, \tag{27}$$

$$v_z(z) = \left(\sum_{k,l} \frac{1}{|v_{zk}(t_l)|} \right)^{-1} \sum_{k,l} \frac{v_{zk}(t_l)}{|v_{zk}(t_l)|}. \tag{28}$$

The second way of sampling is labelled as 'sampling in boxes'. According to this method, the abscissa z is divided into a large number of small boxes Δz wide and infinite over perpendicular axes. Any property may be defined in the jth box (i.e. between $z_j - \Delta z/2$ and $z_j + \Delta z/2$) as

$$\begin{aligned} \langle \xi \rangle_j &= \left(\frac{1}{\Delta z} \int_{z_j - \Delta z/2}^{z_j + \Delta z/2} f_{\mathrm{SST}}(z, \boldsymbol{v})\, \mathrm{d}\boldsymbol{r}\, \mathrm{d}\boldsymbol{v} \right)^{-1} \\ &\quad \times \frac{1}{\Delta z} \int_{z_j - \Delta z/2}^{z_j + \Delta z/2} \xi f_{\mathrm{SST}}(z, \boldsymbol{v})\, \mathrm{d}\boldsymbol{r}\, \mathrm{d}\boldsymbol{v} \\ &\approx \left(\sum_{k=1}^{N} \Delta t_k^j \right)^{-1} \sum_{k=1}^{N} \xi_k^j \Delta t_k^j, \end{aligned} \tag{29}$$

where $f_{\mathrm{SST}}(z, \boldsymbol{v})$ is the steady state distribution function, ξ_k^j is the value of the quantity to be sampled when the kth electron is contained in the jth box, Δt_k^j is the residence time of the electron in that box and N is the total number of electrons which appear there. Electrons moving towards both the cathode and the anode must be considered and sampled. The reasons why the residence time of the electrons must be considered in the above sampling formula are given in [42]. These two sampling techniques must yield the same results under the same physical conditions in simulation. Both sampling techniques provide spatial variation of transport properties with high spatial resolution. If it is not otherwise specified, in this work the spatially resolved transport properties are obtained via box sampling. The internal consistency between membrane and box sampling has been checked and found to be very good.

The spatially resolved rate coefficients can be calculated by determining the number of collisions of type m in the jth spatial box located at z_j [45]:

$$\frac{R^m(z_j)}{n_0} = \frac{N_j^m}{\Delta z N_{\mathrm{e}}(z_j)}, \tag{30}$$

where N_j^m denotes the number of collisions m, Δz is the width of the box and $N_{rme}(z_j)$ represents the net number of residential electrons. This procedure is similar to the actual experimental measurements of spatially resolved excitation and ionization coefficients [45]. Some tests of the procedure have been made by comparing the ionization rate coefficients obtained from the slope of the simulated spatial profile of electron emission and by direct sampling (30) with the results produced by integrating the EEDF and the corresponding cross section. In a similar fashion excitation coefficients that may be sampled in the Monte Carlo simulation at any point may be compared with the integrals of the corresponding cross sections and also compared with the experimental excitation coefficient that may be determined only at the anode. The comparisons of the data obtained from simulations by the two different techniques always gave data that were in good agreement and were an important check of internal consistency especially important if we extend the technique to the non-hydrodynamic situation.

3.4. On the calculation of coefficients in the hydrodynamic expansion

The question that concerns us in this work is the calculation of the expansion coefficients in the density gradient expansion of the transport properties, which are determined from the tensor functions $f^{(s)}(\boldsymbol{v})$. In order to find these functions we follow the previous works of Kumar *et al* [39], Kumar [65] and Nolan *et al* [62]. We will consider the most general situation, of which the SST case is one limiting case. By doing so, the following tensor functions of rank k may be introduced:

$$N^{(k)} = \int n(\boldsymbol{r}, t) \frac{(\boldsymbol{r})^k}{k!}\, \mathrm{d}\boldsymbol{r} = \int F^{(k)}(\boldsymbol{v})\, \mathrm{d}\boldsymbol{v}, \tag{31}$$

$$F^{(k)}(\boldsymbol{v}) = \int f(\boldsymbol{r}, \boldsymbol{v}) \frac{(\boldsymbol{r})^k}{k!}\, \mathrm{d}\boldsymbol{r}. \tag{32}$$

Although these quantities have a clear physical interpretation they cannot be measured in experiments. However, these quantities can be calculated in Monte Carlo simulations. Taking successive moments of the electron number density under SST conditions we have:

$$N^{(0)} = \int n(\boldsymbol{r},t)\,\mathrm{d}\boldsymbol{r} = \int F^{(0)}(\boldsymbol{v})\,\mathrm{d}\boldsymbol{v} \equiv N, \tag{33}$$

$$N^{(1)} = \int \boldsymbol{r} n(\boldsymbol{r},t)\,\mathrm{d}\boldsymbol{r} = \int F^{(1)}(\boldsymbol{v})\,\mathrm{d}\boldsymbol{v} \equiv N\langle \boldsymbol{r}\rangle, \tag{34}$$

$$N^{(2)} = \int \frac{1}{2} r^2 n(\boldsymbol{r},t)\,\mathrm{d}\boldsymbol{r} = \int F^{(2)}(\boldsymbol{v})\,\mathrm{d}\boldsymbol{v} \equiv \frac{1}{2} N\langle \boldsymbol{rr}\rangle, \tag{35}$$

where N is the total number of electrons at any time t and the angular brackets denote the averages over all electrons at any moment t. Substitution of (4) into (32) and using (33)–(35) yield the following expressions for the lowest $F^{(k)}(\boldsymbol{v})$ tensors:

$$F^{(0)}(\boldsymbol{v}) = Nf^{(0)}(\boldsymbol{v}), \tag{36}$$

$$F^{(1)}(\boldsymbol{v}) = Nf^{(0)}(\boldsymbol{v})\langle \boldsymbol{r}\rangle + Nf^{(1)}(\boldsymbol{v}), \tag{37}$$

$$F^{(2)}(\boldsymbol{v}) = \tfrac{1}{2} N\langle \boldsymbol{rr}\rangle f^{(0)}(\boldsymbol{v}) + \tfrac{1}{2} N\left[\langle \boldsymbol{r}\rangle f^{(1)}(\boldsymbol{v}) + f^{(1)}(\boldsymbol{v})\langle \boldsymbol{r}\rangle\right] + Nf^{(2)}(\boldsymbol{v}). \tag{38}$$

It is easily seen that the tensor functions $f^{(s)}(\boldsymbol{v})$ are given by

$$f^{(0)}(\boldsymbol{v}) = \frac{1}{N}\int f(\boldsymbol{r},\boldsymbol{v},t)\,\mathrm{d}\boldsymbol{r}, \tag{39}$$

$$f^{(1)}(\boldsymbol{v}) = \frac{1}{N}\int \boldsymbol{r} f\,(\boldsymbol{r},\boldsymbol{v},t)\,\mathrm{d}\boldsymbol{r} - \frac{1}{N}\int f(\boldsymbol{r},\boldsymbol{v},t)\,\mathrm{d}\boldsymbol{r}\frac{1}{N}\int \boldsymbol{r} f(\boldsymbol{r},\boldsymbol{v},t)\,\mathrm{d}\boldsymbol{r}\,\mathrm{d}\boldsymbol{v}, \tag{40}$$

$$f^{(2)}(\boldsymbol{v}) = \frac{1}{2N}\int \boldsymbol{rr} f(\boldsymbol{r},\boldsymbol{v},t)\,\mathrm{d}\boldsymbol{r} - \frac{1}{2N}\int \boldsymbol{rr} f(\boldsymbol{r},\boldsymbol{v},t)\,\mathrm{d}\boldsymbol{r}\,\mathrm{d}\boldsymbol{v}\frac{1}{N}\int f(\boldsymbol{r},\boldsymbol{v},t)\,\mathrm{d}\boldsymbol{r} - \frac{1}{N}\int \boldsymbol{r} f(\boldsymbol{r},\boldsymbol{v},t)\,\mathrm{d}\boldsymbol{r}\,\mathrm{d}\boldsymbol{v}\frac{1}{N}\int \boldsymbol{r} f(\boldsymbol{r},\boldsymbol{v},t)\,\mathrm{d}\boldsymbol{r} + \frac{1}{N}\int f(\boldsymbol{r},\boldsymbol{v},t)\,\mathrm{d}\boldsymbol{r}\left[\frac{1}{N}\int \boldsymbol{r} f(\boldsymbol{r},\boldsymbol{v},t)\,\mathrm{d}\boldsymbol{r}\,\mathrm{d}\boldsymbol{r}\right]^2. \tag{41}$$

Under an infinite plane parallel configuration, with the electric field in the z-direction, the spatial variations are along the z axis only, with no variations along the x- or y-directions.

Substitution of (39)–(41) into (9) allows us to determine the expansion coefficients in the density gradient expansion of the particle flux, or equivalently the flux transport coefficients:

$$\Gamma_0 = \langle v_z\rangle \equiv W^{(\star)}, \tag{42}$$

$$\Gamma_1 = \langle z v_z\rangle - \langle z\rangle\langle v_z\rangle \equiv D_{\mathrm{L}}^{(\star)}, \tag{43}$$

$$\Gamma_2 = \tfrac{1}{2}\langle z^2 v_z\rangle - \tfrac{1}{2}\langle z^2\rangle\langle v_z\rangle - \langle z\rangle\langle z v_z\rangle + \langle z\rangle^2\langle v_z\rangle. \tag{44}$$

Expressions (42) and (43) independently confirm the validity of using (11) and (12) in the calculation of the flux drift and flux longitudinal diffusion coefficients. Equation (41) allows us to calculate higher order flux terms.

Likewise, substitution of (39)–(41) into (8), respectively, allows us to determine the coefficients in the density gradient expansion of the average energy:

$$\varepsilon_0 = \tilde{\varepsilon}, \tag{45}$$

$$\varepsilon_1 = \frac{1}{2}\langle z\varepsilon\rangle - \langle z\rangle\langle\varepsilon\rangle = -\frac{\gamma}{n}, \tag{46}$$

$$\varepsilon_2 = \tfrac{1}{2}\langle z^2\varepsilon\rangle - \tfrac{1}{2}\langle z^2\rangle\langle\varepsilon\rangle - \langle z\rangle\langle z\varepsilon\rangle + \langle z\rangle^2\langle\varepsilon\rangle. \tag{47}$$

Relations (42)–(47) provide a method in MC simulations for easily sampling the expansion coefficients in the density gradient expansion of both the average energy and electron flux.

In summary, we now have the tools to calculate using a MC simulation:

- spatial profiles of the transport properties for the SST experiment;
- bulk and flux transport coefficients under hydrodynamic conditions;
- expansion coefficients in the density gradient expansion of the transport properties including the gradient energy parameter.

We are then in a position to assess the accuracy/convergence of the density gradient expansion for the SST average energy and SST average velocity in the far-down stream SST profiles where hydrodynamic conditions generally prevail.

4. Results and discussion

4.1. The ionization Lucas–Saelee model

To understand the fundamental effects of ionization on spatial relaxation profiles of the electron transport properties we consider electrons in the ionization Lucas–Saelee model [66]. The details of this model gas are

$$\sigma_{\mathrm{e}}(\epsilon) = 4\epsilon^{-1/2}\ \text{Å}^2,$$

$$\sigma_{\mathrm{ex}}(\epsilon) = \begin{cases} 0.1(1-F)(\epsilon - 15.6)\ \text{Å}^2, & \epsilon \geqslant 15.6\,\text{eV}, \\ 0, & \epsilon < 15.6\,\text{eV}, \end{cases}$$

$$\sigma_{\mathrm{I}}(\epsilon) = \begin{cases} 0.1F(\epsilon - 15.6)\ \text{Å}^2, & \epsilon \geqslant 15.6\,\text{eV}, \\ 0, & \epsilon < 15.6\,\text{eV}, \end{cases} \tag{48}$$

where σ_{e}, σ_{ex} and σ_{I} are the cross sections for elastic, inelastic and ionization collisions, respectively. Other details of the model include $\epsilon_i = 15.6\,\text{eV}$, $T_0 = 0\,\text{K}$, $E/n_0 = 10\,\text{Td}$ ($1\,\text{Td} = 10^{-21}\,\text{V m}^2$), $m/M = 10^{-3}$, where m and M denote the electron and molecular mass, respectively, while T_0 is the temperature of the background gas.

There are some interesting aspects associated with this model. Firstly, the sum of the inelastic and ionization cross sections is independent of the parameter F, while secondly the threshold energies are the same for both processes. Thus, this model can be used to isolate and separate effects of inelastic and ionization collisions, respectively. This can be done through the variation of a parameter F. However, it is common in the literature on electron swarms to find ionization processes simply as another inelastic process [10]. If this scenario was

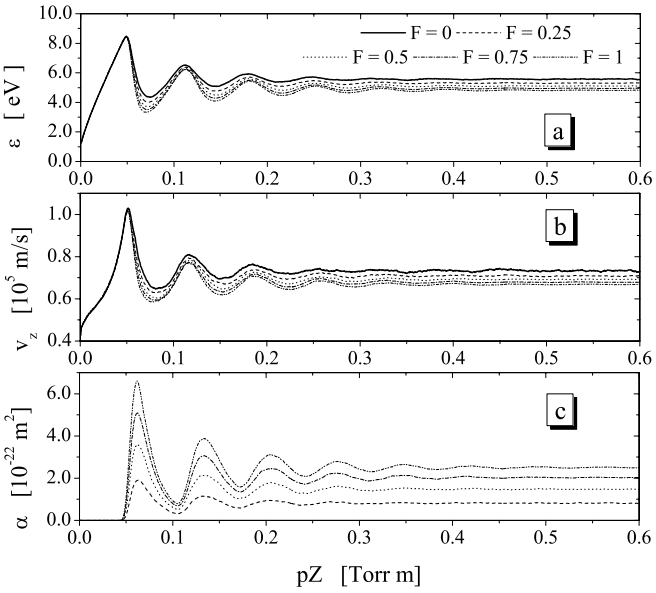

Figure 1. Spatial relaxation of the (*a*) mean energy, (*b*) average velocity and (*c*) ionization rate coefficient for the ionization model of Lucas and Saelee at $E/n_0 = 10$ Td. The initial electron energy is 1.5 eV.

used in our simulations there would be no variation in the calculated transport properties with respect to variation in the parameter F. In addition, as detailed earlier, $\varepsilon_{\rm SST}$ and $v_{\rm SST}$ reduce to $\tilde{\varepsilon}$ and $W^{(\star)}$, respectively. One should bear this in mind in the following discussion.

In figure 1, we display spatial relaxation of the mean energy, average velocity and ionization rate coefficient, respectively, for different values of F. We observe periodic relaxation profiles for all the conditions considered and this behaviour is consistent with previous results published by Li *et al* [28][3]. The average energy does not depend on F near the cathode region, reflecting the distance required for electrons emitted at the initial energy to obtain sufficient energy to initiate ionization collisional processes. Figure 1(*c*) shows spatial relaxation of the ionization rate. As expected, the ionization rate increases when increasing the parameter F. In the region near the cathode the ionization rate is significantly reduced and it begins rapidly to grow after electrons travel enough long distance sufficient for their energy to be higher than the ionization threshold. The ionization rate peaks at the positions which correspond to the peaks of the mean energy. The explanation for this is associated with the fact that the ionization collision frequency increases with energy for this model and consequently electrons undergo more ionization collisions at higher energy.

Spatial relaxation can be characterized by a spatial relaxation length and a relaxation period if oscillatory behaviour exists. The detailed calculations of the positions of the extremes in transport properties for the Lucas–Saelee model revealed a small increase in the periods of oscillations of the various transport properties when increasing F. In addition, it has been observed that the relaxation periods are

[3] An error exists in the results presented in [28] arising from an incorrect implementation of the boundary at infinity in the computer code.

Table 1. Comparison between the SST and mean energies, as well as accuracy of the low-order truncations of the density gradient expansion for the ionization model of Lucas and Saelee.

	$F=0$	$F=0.25$	$F=0.5$	$F=0.75$	$F=1$
$\tilde{\varepsilon}$ (eV)	5.57	5.39	5.22	5.09	4.97
$\varepsilon_{\rm SST}$ (eV)	5.57	5.30	5.11	4.95	4.82
Δ (%)	0.0	1.7	2.1	2.75	3.0
$\alpha\varepsilon_1$ (eV)	0.00	0.07	0.11	0.13	0.13
ε_0–$\alpha\varepsilon_1$ (eV)	5.57	5.32	5.11	4.96	4.84
Δ (%)	0.0	0.4	0.0	0.2	0.4

Table 2. Comparison between the SST and flux drift velocities, as well as accuracy of the low-order truncations of the density gradient expansion for the ionization model of Lucas and Saelee.

	$F=0$	$F=0.25$	$F=0.5$	$F=0.75$	$F=1$
$W^{(\star)}$ (10^4 m s^{-1})	7.32	7.32	7.32	7.32	7.32
$v_{\rm SST}$ (10^4 m s^{-1})	7.32	7.08	6.92	6.79	6.68
Δ (%)	0.0	3.3	5.5	7.2	8.7
$\alpha\Gamma_1$ (10^3 m s^{-1})	0.00	2.32	4.05	5.40	6.53
Γ_0–$\alpha\Gamma_1$ (10^4 m s^{-1})	7.32	7.09	6.92	6.78	6.67
Δ (%)	0.0	0.1	0.0	0.1	0.1

approximately one and a half times longer than the theoretical value which can be easily calculated through $\Delta z = \varepsilon_{\rm i}/eE$, where $\varepsilon_{\rm i}$ is the threshold for inelastic cross section, e is the electron charge and E is the magnitude of the electric field. Figures 1(*a*)–(*c*) also demonstrate that the relaxation lengths of all transport properties increase with the parameter F. These results independently confirm the previous calculations and the reader is referred to [28] for details.

In what follows we restrict our discussion to the stage of evolution in the SST experiment where the average energy and average velocity have relaxed to their spatially independent values $\varepsilon_{\rm SST}$ and $v_{\rm SST}$. We can see immediately from tables 1 and 2 that the SST values disagree with the mean energy and flux drift velocities traditionally determined in hydrodynamic calculations. As expected, from tables 1 and 2 we observe that for $F = 0$, when conservative collisions are operative only, $\varepsilon_{\rm SST}$ and $v_{\rm SST}$ reduce to $\tilde{\varepsilon}$ and $W^{(\star)}$, respectively. While there are no/minimal variations in $W^{(\star)}$ with increasing F, the $\tilde{\varepsilon}$ decreases with increasing F [62]. For SST conditions, both the $\varepsilon_{\rm SST}$ and the $v_{\rm SST}$ decrease with F. This is illustrated in figures 1 and 2.

A striking feature of the data presented in tables 1 and 2 is a small but noticeable discrepancy between $\varepsilon_{\rm SST}$ and $\tilde{\varepsilon}$, and $v_{\rm SST}$ with $W^{(\star)}$ as F increases. In addition, it is clearly evident that the differences between $v_{\rm SST}$ with $W^{(\star)}$ are more affected by a parameter F (the degree of ionization) than the differences between the $\varepsilon_{\rm SST}$ and $\tilde{\varepsilon}$. For the highest ionization degree of $F = 1$, the differences between $v_{\rm SST}$ with $W^{(\star)}$ approaches 10%. These properties are quite general when ionization is involved, i.e.

- the SST average velocity is always less than the flux drift velocity, and

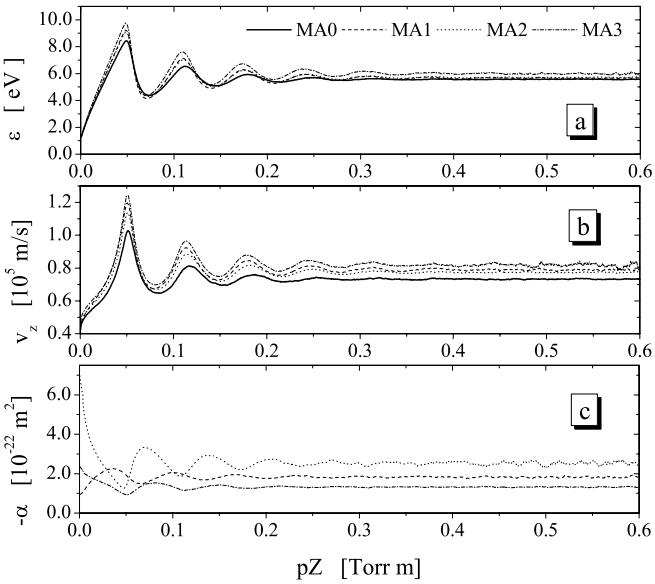

Figure 2. Spatial relaxation of the (*a*) mean energy, (*b*) average velocity and (*c*) ionization rate coefficient for modified attachment model of Ness and Robson at $E/n_0 = 10$ Td. The initial electron energy is 1.5 eV.

- the SST average energy is always less than the mean energy.

One can immediately see that these are general properties by referring to relations (16) and (17). For example, from (17) and using the fact that both D_L and α are positive it follows immediately that $v_{SST} < W^{(\star)}$. Likewise, from (16) since γ (or ε_1) is always negative [55] and α is positive for ionization, it then follows that $\varepsilon_{SST} < \tilde{\varepsilon}$.

Physically (to first order in density gradients), the flux of electrons in the SST experiment is a combination of the drift due to the electric field force ($nW^{(\star)}$) and a diffusive flux due to gradients in the electron density profile ($-D_L dn/dz$). When ionization processes are dominant in the SST experiment, the density profile increases exponentially with distance in the direction of the electric field force. Hence, the diffusive flux arising from this gradient in the electron number density is then in the *opposite* direction to the drifted flux due to the electric field. It then follows that the diffusive flux acts to reduce the field flux and hence $v_{SST} < W^{(\star)}$.

Likewise (to first order in density gradients) the average energy of electrons is a combination of the mean energy $\tilde{\varepsilon}$ and a contribution associated with the energy losses/gains due to diffusive processes ($\gamma dn/dz$). The mean energy of electrons far from the source is a balance of energy deposited by the field and that dissipated in collisions. As electrons move away from the source they fall through a greater potential and hence have more energy deposited by field. Now considering the contribution to the average energy associated with the diffusive flux electrons: since this diffusive flux is against the electric field force (due to the increasing electron density profile) these electrons are going against the field force and this contribution is acting to reduce the average energy. It then follows that $\varepsilon_{SST} < \tilde{\varepsilon}$.

Table 3. Comparison between the SST and mean energies, as well as accuracy of the low-order truncations of the density gradient expansion for the modified attachment model of Ness and Robson.

	MA0	MA1	MA2	MA3
$\tilde{\varepsilon}$ (eV)	5.57	5.45	5.57	5.73
ε_{SST} (eV)	5.57	5.66	5.71	6.04
Δ (%)	0.0	3.7	2.5	5.1
$\alpha\varepsilon_1$ (eV)	0.00	0.21	0.14	0.28
ε_0–$\alpha\varepsilon_1$ (eV)	5.57	5.66	5.71	6.01
Δ (%)	0.0	0.0	0.0	0.2

4.2. Modified attachment model of Ness and Robson

To investigate spatial relaxation in the presence of the electron attachment, the modified Ness–Robson attachment model has been considered. The details of this gas model are [62]:

$$\sigma_e(\epsilon) = 4\epsilon^{-1/2}\ \text{Å}^2,$$

$$\sigma_{ex}(\epsilon) = \begin{cases} 0.1(1-F)(\epsilon - 15.6)\ \text{Å}^2, & \epsilon \geqslant 15.6\,\text{eV}, \\ 0, & \epsilon < 15.6\,\text{eV}, \end{cases}$$

$$\sigma_a = a\epsilon^p\ \text{Å}^2, \tag{49}$$

where the threshold for the excitation is $\epsilon_i = 15.6$ eV, $T_0 = 0$ K, $E/n_0 = 10$ Td (1 Td $= 10^{-21}$ V m^{-2}), $m/M = 10^{-3}$, where m and M denote the electron and molecular mass, respectively, while T_0 is the temperature of the background gas (table 3). In this model the parameters a and p control the magnitude and the energy dependence of the attachment cross section, respectively. This paper considers zero attachment model (MA0: $a = 0$, $p = 0$) and the case studies where the attachment cross section is proportional to the electron velocity (MA1: $a = 5\times10^{-4}$, $p = 0.5$), inversely proportional to the electron velocity (MA2: $a = 2\times10^{-3}$, $p = -0.5$) and inversely proportional to the electron energy (MA3: $a = 8\times10^{-3}$, $p = -1.0$) [62]. In figure 2 we demonstrate the spatial relaxation of the average energy, average velocity and attachment rate coefficient. They display the same general behaviour in the relaxation profiles as those for ionization. The only noticeable differences arise from the difference in the thresholds for the ionization and attachment models. For the attachment model, the threshold is zero and hence the average energy and average velocity deviate from the conservative case in the close vicinity of the cathode. In the regime where the transport properties have relaxed to spatially independent values, the following important general properties for attachment in SST are observed:

- the SST drift velocity is always greater than the flux drift velocity, and
- the SST average energy is always greater than the mean energy.

Using similar arguments to that outlined for ionization, but with our arguments modified with α now being negative, these general properties can be inferred from relations (16) and (17) (table 4). Physically, when attachment is the dominant non-conservative process, the diffusive flux contribution to the average velocity of the electrons is now in the direction of the directed flux $W^{(\star)}$ since the density profile decreases

Table 4. Comparison between the SST and flux drift velocities, as well as accuracy of the low-order truncations of the density gradient expansion for the ionization model of Lucas and Saelee.

	MA0	MA1	MA2	MA3
$W^{(\star)}$ (10^4 m s^{-1})	7.32	7.32	7.32	7.32
$v_{\rm SST}$ (10^4 m s^{-1})	7.32	7.89	7.72	8.17
Δ (%)	0.0	7.2	5.2	10.4
$\alpha\Gamma_1$ (10^3 m s^{-1})	0.00	5.27	3.82	7.68
Γ_0–$\alpha\Gamma_1$ (10^4 m s^{-1})	7.32	7.85	7.70	8.09
Δ (%)	0.0	0.5	0.3	1.0

exponentially with distance from the source. It then follows that the diffusive flux acts to enhance the field flux and hence $v_{\rm SST} > W^{(\star)}$. Likewise, since the diffusive flux is in the direction of the field force, the contribution to the average energy associated with diffusive processes is now positive, and it follows that $\varepsilon_{\rm SST} > \tilde{\varepsilon}$.

5. Conclusion

In this paper we have developed a Monte Carlo simulation technique to consider the spatial relaxation of electrons for an idealized SST experiment. The study has focused on the explicit influence of non-conservative collisional processes on the relaxation behaviour, and some important and quite general properties associated with the impact of attachment/ionization have emerged from this study. Also in this paper we have considered the convergence of the density gradient expansion often used in the hydrodynamic analysis of swarm experiments. To do this, we have developed a technique that allows us to accurately calculate expansion coefficients in the density gradient expansion using the Monte Carlo technique. We were able to demonstrate for the cases considered that when hydrodynamic conditions prevailed the density gradient expansion converged rapidly. Convergence to within 1.0% is achieved in the SST properties using only the first two terms in the expansion. While one could expect that these effects will be of importance for electrons only, recently evidence of the influence of the non-conservative processes on transport of ions [67] and positrons [68] were found and discussed. In the case of ions the mean energies for them to occur are quite large but still within the range of practical discharges. In the case of positrons extraordinarily high effects were found which may yield an interest in performing analysis like the one reported here.

Acknowledgments

All of the authors would like to acknowledge the support of the Australian Research Council and the Centre for Antimatter-Matter studies. Two of the authors (SD and ZLjP) were partly funded by the MNTR project 141025. It is a pleasure to acknowledge the helpful discussions with Professor Robert Robson, Dr Bo Li and Dr Zoran Raspopović.

References

[1] Makabe T and Petrović Z Lj 2006 *Plasma Electronics: Applications in Microelectronic Device Fabrication* (New York: Taylor and Francis Group)
[2] Boeuf J P and Marode E 1982 *J. Phys. D: Appl. Phys.* **15** 2169
[3] Kim J B, Kawamura K, Choi Y W, Browden M D and Muraoka K 1999 *IEEE Trans. Plasma Sci.* **27** 1510
[4] Petrović Z Lj, Raspopović Z M, Dujko S and Makabe T 2002 *Appl. Surf. Sci.* **192** 1
[5] Petrović Z Lj, Šuvakov M, Nikitović Ž, Dujko S, Šašić O, Jovanović J, Malović G and Stojanović V 2007 *Plasma Sources Sci. Technol.* **16** S1–12
[6] Kortshagen U, Busch C and Tsendin L D 1996 *Plasma Sources Sci. Technol.* **5** 1
[7] Winkler R and Sigeneger F 2001 *J. Phys. D: Appl. Phys.* **34** 3407
[8] Winkler R, Sigeneger F and Uhrlandt D 1996 *Pure Appl. Chem.* **68** 1065
[9] Sigeneger F and Winkler R 1997 *Plasma Chem. Plasma Process.* **17** 1
[10] Sigeneger F and Winkler R 1997 *Plasma Chem. Plasma Process.* **17** 281
[11] Winkler R, Petrov G, Sigeneger F and Uhrlandt D 1997 *Plasma Sources Sci. Technol.* **6** 118
[12] Loffhagen D, Sigeneger F and Winkler R 2003 *Plasma Chem. Plasma Process.* **23** 415
[13] Sigeneger F, Golubovskii Yu B, Porokhova I A and Winkler R 1998 *Plasma Chem. Plasma Process.* **18** 153
[14] Sigeneger F and Winkler R 2000 *Plasma Chem. Plasma Process.* **20** 429
[15] Sigeneger F, Sukhinin G I and Winkler R 2000 *Plasma Chem. Plasma Process.* **20** 87
[16] Sigeneger F and Winkler R 1995 *Phys. Rev.* E **52** 3281
[17] Arndt S, Uhrlandt D and Winkler R 2000 *J. Phys. D: Appl. Phys.* **34** 1982
[18] Uhrlandt D and Winkler R 1996 *J. Phys. D: Appl. Phys.* **29** 115
[19] Petrov G and Winkler R 1997 *J. Phys. D: Appl. Phys.* **30** 53
[20] Petrov G and Winkler R 1998 *Plasma Chem. Plasma Process.* **18** 113
[21] Hannemann M, Hardt P, Loffhagen D, Schmidt M and Winkler R 2000 *Plasma Sources Sci. Technol.* **9** 387
[22] Loffhagen D, Sigeneger F and Winkler R 2002 *J. Phys. D: Appl. Phys.* **35** 1768
[23] Golubovskii Yu B, Porokhova I A, Behnke J and Nekutchaev V O 1998 *J. Phys. D: Appl. Phys.* **31** 2447
[24] Golubovskii Yu B, Maiorov V A, Porokhova I A and Behnke J 1999 *J. Phys. D: Appl. Phys.* **32** 1391
[25] Golubovskii Yu B, Kozakov R V, Maiorov V A, Behnke J and Behnke J F 2000 *Phys. Rev.* E **62** 2707
[26] Golubovskii Yu B, Skoblo A Yu, Maiorov V A and Nekutchaev V O 2002 *Plasma Sources Sci. Technol.* **11** 309
[27] White R D, Robson R E, Schmidt B and Morrison M A 2003 *J. Phys. D: Appl. Phys.* **36** 3125
[28] Li B, White R D and Robson R E 2002 *J. Phys. D: Appl. Phys.* **35** 2914
[29] Loffhagen D 2005 *Plasma Chem. Plasma Process.* **25** 519
[30] Winkler R, Maiorov V A and Sigeneger F 2000 *J. Appl. Phys.* **87** 2708
[31] Li B, Robson R E and White R D 2006 *Phys. Rev.* E **74** 026405
[32] Winkler R, Loffhagen D and Sigeneger F 2002 *Appl. Surf. Sci.* **192** 50
[33] Robson R E, Li B and White R D 2000 *J. Phys. B: At. Mol. Opt. Phys.* **33** 507
[34] Sigeneger F, Winkler R and Robson R E 2003 *Contrib. Plasma. Phys.* **43** 178
[35] Holst G and Oosterhuis E 1921 *Physica* **1** 78
[36] Fletcher J 1985 *J. Phys. D: Appl. Phys.* **18** 221

[37] Malović G N, Božin J V, Jelenković B M and Petrović Z Lj 1999 *Eur. Phys. J.* D **7** 129
[38] Malović G N, Strinić A I, Petrović Z Lj, Božin J V and Manola S S 2000 *Eur. Phys. J. D* **10** 147
[39] Kumar K, Skullerud H R and Robson R E 1980 *Aust. J. Phys.* **33** 343
[40] Malović G , Strinić A, Živanov S, Marić D and Petrović Z Lj 2003 *Plasma Source Sci. Technol.* **12** S1
[41] Thomas R W L and Thomas W R L 1969 *J. Phys. B: At. Mol. Phys.* **2** 562
[42] Sakai Y, Tagashira H and Sakamoto S 1972 *J. Phys. B: At. Mol. Phys.* **5** 1010
[43] Sakai Y, Tagashira H and Sakamoto S 1977 *J. Phys. D: Appl. Phys.* **10** 1035
[44] Boeuf J P and Marode E 1984 *J. Phys. D: Appl. Phys.* **17** 1133
[45] Stojanović V D and Petrović Z Lj 1998 *J. Phys. D: Appl. Phys.* **31** 834
[46] Petrović Z Lj and Stojanović V D 1998 *J. Vac. Sci. Technol.* A **16** 329
[47] Sommerer T J, Hitchion W N G and Lauler J E 1989 *Phys. Rev.* A **39** 6356
[48] Sugawara H, Sakai Y and Tagashira H 1992 *J. Phys. D: Appl. Phys.* **25** 1483
[49] Sugawara H, Sakai Y and Tagashira H 1994 *J. Phys. D: Appl. Phys.* **27** 90
[50] Takeda A and Ikuta N 1997 *J. Phys. Soc. Japan* **66** 1672
[51] Kortshagen U, Parker G J and Lawler J E 1996 *Phys. Rev.* E **54** 6746
[52] Dyatko N A and Napartovich A P 1999 *J. Phys. D: Appl. Phys.* **32** 3169
[53] Sigeneger F, Dyatko N A and Winkler R 2003 *Plasma Chem. Plasma Process.* **23** 103
[54] Dujko S, Raspopović Z M and Petrović Z Lj 2005 *J. Phys. D: Appl. Phys.* **38** 2952
[55] White R D, Robson R E and Ness K F 1995 *Aust. J. Phys.* **48** 925
[56] Robson R E 1991 *Aust. J. Phys.* **44** 685
[57] Blevin H A and Fletcher J 1984 *Aust. J. Phys.* **37** 593
[58] Tagashira H, Sakai Y and Sakamoto S 1977 *J. Phys. D: Appl. Phys.* **10** 1051
[59] Vrhovac S B, Stojanović V D, Jelenković B M and Petrović Z Lj 2001 *J. Appl. Phys.* **90** 5871
[60] Skullerud H R 1968 *J. Phys. D: Appl. Phys.* **1** 1567
[61] Itoh H and Musha T 1960 *J. Phys. Soc. Japan* **15** 1675
[62] Nolan A M, Brennan M J, Ness K F and Wedding A B 1997 *J. Phys. D: Appl. Phys.* **30** 2865
[63] Dujko S, White R D, Ness K F, Petrović Z Lj and Robson R E 2006 *J. Phys. D: Appl. Phys.* **39** 4788
[64] Robson R E, White R D and Petrović Z Lj 2005 *Rev. Mod. Phys.* **77** 1304
[65] Kumar K 1981 *J. Phys. D: Appl. Phys.* **14** 2199
[66] Lucas J and Saelee H 1975 *J. Phys. D: Appl. Phys.* **8** 640
[67] Petrović Z Lj, Raspopović Z M, Stojanović V D, Jovanović J V, Malović G, Makabe T and de Urquijo J 2007 *Appl. Surf. Sci.* **253** 6619
[68] Šuvakov M, Petrović Z Lj, Marler J P, Buckman S J, Robson R E and Malović G 2008 *New J. Phys.* **10** 053034